Detailed Investigation of the Self-Aggregation of Convection in Cloud-Resolving Simulations

CAROLINE J. MULLER

Atmospheric and Oceanic Sciences Program, Princeton University, Princeton, New Jersey

ISAAC M. HELD

NOAA/Geophysical Fluid Dynamics Laboratory, Princeton, New Jersey

ABSTRACT

In models of radiative–convective equilibrium it is known that convection can spontaneously aggregate into one single localized moist region if the domain is large enough. The large changes in the mean climate state and radiative fluxes accompanying this self-aggregation raise questions as to what simulations at lower resolutions with parameterized convection, in similar homogeneous geometries, should be expected to produce to be considered successful in mimicking a cloud-resolving model.

The authors investigate this self-aggregation in a nonrotating, three-dimensional cloud-resolving model on a square domain without large-scale forcing. It is found that self-aggregation is sensitive not only to the domain size, but also to the horizontal resolution. With horizontally homogeneous initial conditions, convective aggregation only occurs on domains larger than about 200 km and with resolutions coarser than about 2 km in the model examined. The system exhibits hysteresis, so that with aggregated initial conditions, convection remains aggregated even at our finest resolution, 500 m, as long as the domain is greater than 200–300 km.

The sensitivity of self-aggregation to resolution and domain size in this model is due to the sensitivity of the distribution of low clouds to these two parameters. Indeed, the mechanism responsible for the aggregation of convection is the dynamical response to the longwave radiative cooling from low clouds. Strong longwave cooling near cloud top in dry regions forces downward motion, which by continuity generates inflow near cloud top and near-surface outflow from dry regions. This circulation results in the net export of moist static energy from regions with low moist static energy, yielding a positive feedback.

1. Introduction

It is well known that convection can organize on a wide range of scales. Important examples of organized convection include squall lines, mesoscale convective systems (Emanuel 1994; Holton 2004), and the Madden–Julian oscillation (Grabowski and Moncrieff 2004). The ubiquity of convective organization above tropical oceans has been pointed out in several observational studies (Houze and Betts 1981; WCRP 1999; Nesbitt et al. 2000).

The spontaneous appearance of convective organization in cloud-resolving models that are forced homogeneously is a useful starting point for theories of convective organization. Organization can involve a wide range of scales, so large domains are needed, yielding high computational costs. Many studies have been limited to two-dimensional domains (Held et al. 1993; Grabowski and Moncrieff 2001, 2002) or three-dimensional domains in channel configurations (Tompkins 2001a; Stephens et al. 2008), although some fully three-dimensional studies have also been conducted (Tompkins and Craig 1998; Tompkins 2001b; Robe and Emanuel 2001; Bretherton et al. 2005).

Various mechanisms can generate and modulate convective organization in homogeneous environments. These include background vertical shear (e.g., Robe and Emanuel 2001) and various internal feedbacks, such as those involving water vapor (e.g., Held et al. 1993; Tompkins 2001a), surface fluxes (e.g., Emanuel 1986), or radiative fluxes (e.g., Stephens et al. 2008). The

---

Corresponding author address: Caroline J. Muller, Princeton University/GFDL, 201 Forrestal Road, Princeton, NJ 08540.
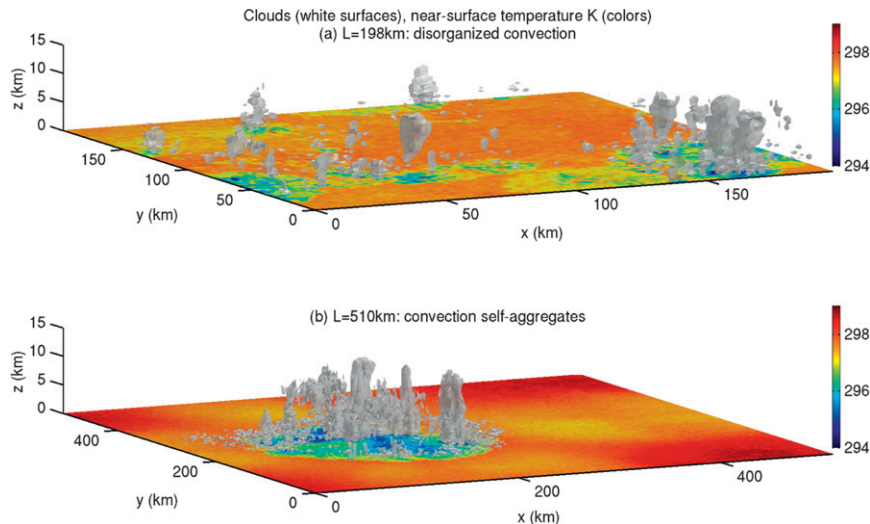E-mail: caroline.muller@noaa.gov

FIG. 1. Instantaneous snapshots of clouds (0.4 g kg^{-1} isosurface of the mixing ratio of all liquid and ice phase condensates, precipitating and nonprecipitating) and near-surface temperature (at the first model level $z = 37.5$ m) after 60 days in two simulations with the same resolution $dx = 2$ km but different domain sizes: $L =$ (a) 198 and (b) 510 km. Convection self-aggregates when the domain is large enough, resulting in an atmospheric state with one convectively active moist region.

organization takes various forms in different studies, such as small-scale banded precipitating systems embedded within mesoscale envelopes (e.g., Tompkins 2001a; Grabowski and Moncrieff 2001) or one single moist region where all of the convection is concentrated (e.g., Held et al. 1993; Bretherton et al. 2005). These differences could be due to the different models used or to differences in the model settings (isotropic domain vs anisotropic channel, presence vs absence of background flow, interactive vs prescribed radiative cooling, interactive vs homogeneous surface fluxes, etc.). The large changes in the mean climate state, radiative fluxes, and climate sensitivity accompanying convective organization raise questions as to what simulations at lower resolutions with parameterized convection, in similar homogeneous geometries, should be expected to produce to be considered successful in mimicking a cloud-resolving model.

Recent studies using a three-dimensional cloud-resolving model show that when the domain is sufficiently large, tropical convection can spontaneously aggregate into one single region, a phenomenon referred to as *self-aggregation* (Bretherton et al. 2005; Emanuel and Khairoutdinov 2010). The final climate is a spatially organized atmosphere composed of two distinct areas: a moist area with intense convection, and a dry area with strong radiative cooling (Figs. 1b and 2b,d). Whether or not a horizontally homogeneous convecting atmosphere in radiative convective equilibrium

self-aggregates seems to depend on the domain size (Bretherton et al. 2005). More generally, the conditions under which this instability of the disorganized radiative convective equilibrium state of tropical convection occurs, as well as the feedback responsible, remain unclear.

Bretherton et al. (2005) pointed out an upgradient transport of moist static energy in the aggregated state, with moist static energy transported from low-energy (dry) to high-energy (moist) regions. (Moist static energy variability is largely dominated by moisture variability due to small horizontal temperature gradients, so that high-energy regions correspond to moist regions). More recently, Emanuel and Khairoutdinov (2010) pointed out hysteresis in the system in simulations where the sea surface temperature (SST) is computed interactively: in their study convection self-aggregates only if the SST is warm enough, but the aggregated convection remains aggregated even if the SST subsequently evolves to unfavorable cold conditions.

In this study, we investigate in detail the onset of self-aggregation and how it depends on various parameters, using essentially the same cloud-resolving model as in Bretherton et al. (2005) and Emanuel and Khairoutdinov (2010). Specifically, the questions that we would like to address are the following:

- How does self-aggregation depend on domain size and resolution?
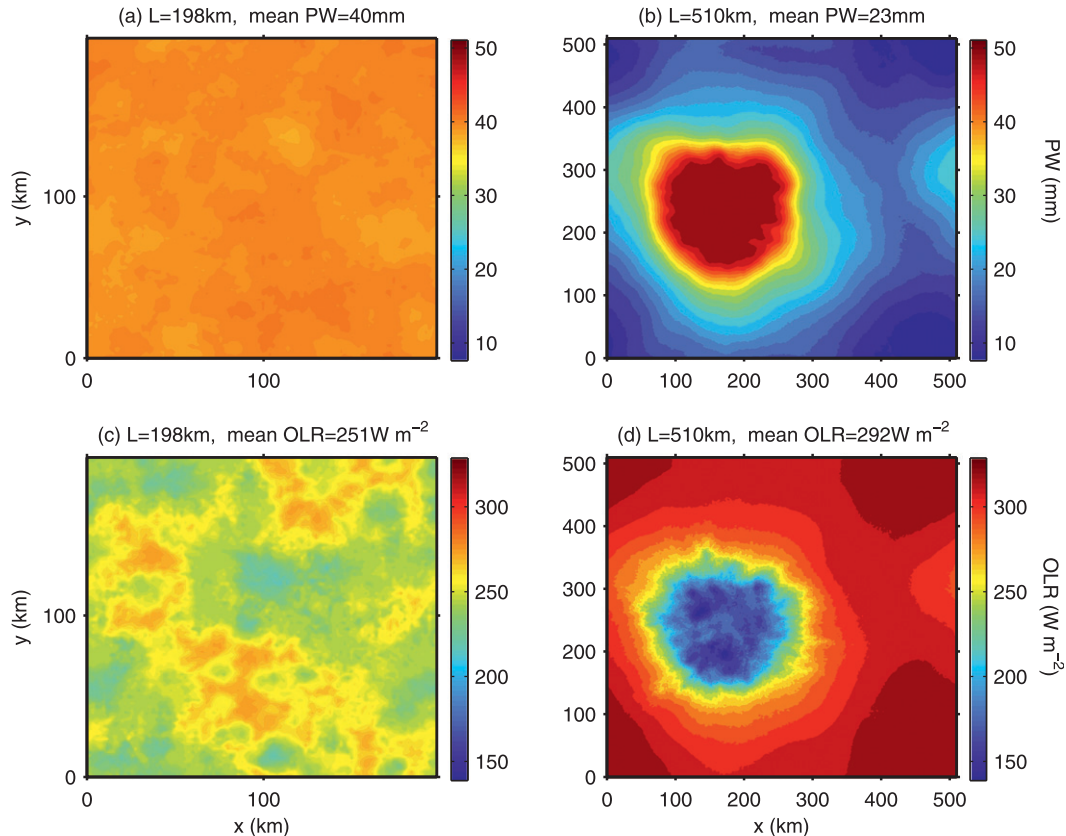- Is there hysteresis?

FIG. 2. Daily mean (a),(b) precipitable water (PW) and (c),(d) outgoing longwave radiation (OLR) after 60 days in two simulations with the same resolution $dx = 2$ km but different domain sizes $L =$ (a),(c) 198 and (b),(d) 510 km. Convection self-aggregates when the domain is large enough (Fig. 1b), resulting in a moist region where convection is concentrated, surrounded by air with very dry conditions and strong longwave cooling.

- What is the feedback responsible for convective aggregation, and how does it explain the sensitivity to domain size and resolution?

The model and the various simulations are discussed in more detail in the next section; section 3 describes the self-aggregated state and its impact on atmospheric properties. The sensitivity of self-aggregation to domain size and resolution is investigated in section 4, while the mechanism responsible for the onset of self-aggregation is discussed in section 5. Concluding remarks are offered in section 6.

2. Numerical simulations

The cloud-resolving model used in this study is a version of the System for Atmospheric Modeling [SAM version 6.6; see Khairoutdinov and Randall (2003) for a full description]. The model solves the anelastic continuity, momentum, and tracer conservation equations. The prognostic thermodynamic variables of the model

are liquid/ice water static energy, total nonprecipitating water (vapor + cloud water + cloud ice), and total precipitating water (rain + snow + graupel). The frozen moist static energy, which is the sum of the liquid/ice water static energy and the total condensate amount times the latent heat of vaporization, is conserved during moist adiabatic processes in the model, including the freezing and melting of precipitation.

All simulations are three-dimensional on a square, doubly periodic horizontal domain with various sizes (typically a few hundred kilometers) and resolutions (from a few hundred meters to a few kilometers). The vertical grid has 64 levels (capped at 27 km with a rigid lid) with the first level at 37.5 m and grid spacing gradually increasing from 80 m near the surface to 400 m above 5 km, and a variable time step (10 s or less to satisfy the Courant–Friedrichs–Lewy condition). To reduce gravity wave reflection and buildup, Newtonian damping is applied to all prognostic variables in the upper third of the model domain. The subgrid-scale (SGS) fluxes are parameterized based on Smagorinsky's

TABLE 1. List of sensitivity runs discussed in section 5.

Run name	Resolution (km)	Domain size (km)	Run description
SFC-homog	Various	Various	Surface fluxes homogenized horizontally at each time step
SW-homog	Various	Various	Shortwave radiative cooling homogenized horizontally at each time step and height
LW-homog	Various	Various	Longwave radiative cooling homogenized horizontally at each time step and height
LWq_v-homog	3.0	381	Surface fluxes, shortwave radiative cooling, and longwave radiative cooling due to water vapor homogenized
LWq_{ci}-zero	3.0	381	Surface fluxes and shortwave radiative cooling homogenized, and contribution from cloud ice to longwave radiative cooling zeroed
LWq_{cl}-zero	3.0	381	Surface fluxes and shortwave radiative cooling homogenized, and contribution from cloud liquid water to longwave radiative cooling zeroed
LWq_{cl}-zero delayed	3.0	381	As in LWq_{cl}-zero, but the contribution from cloud liquid water to longwave radiative cooling is only zeroed after day 10
LW-homog delayed	3.0	381	As in LW-homog, but the longwave radiative cooling is only homogenized horizontally after day 10

eddy diffusivity model, with eddy viscosity and diffusivity coefficients related to the mixing length and the local SGS turbulence kinetic energy (TKE). The former is related to the grid resolution and the local stratification, and the latter is diagnosed from the quasi-steady TKE budget [the same SGS parameterization as in Bretherton et al. (2005) and Emanuel and Khairoutdinov (2010)].

There is no rotation and no diurnal cycle; the latter is removed by using an insolation that is constant in space and time, with exactly the same incident flux and zenith angle as in Tompkins and Craig (1998). The sea surface temperature is fixed and equal to a value of 300 K. There is no imposed background shear, but the horizontally averaged winds are relaxed at all vertical levels over a time scale of 2 h toward zero. We do not expect our qualitative results to be sensitive to this relaxation; in fact, we reproduced some of our runs without the wind relaxation and found that our results on the onset of self-aggregation are not affected: the same runs self-aggregate, but the domain-averaged winds are stronger once aggregation occurs.

The longwave and shortwave radiative cooling rates are computed using the radiation code from the National Center for Atmospheric Research (NCAR) Community Atmosphere Model version 3 (CAM3; Collins et al. 2006). Note that this is a slightly different version than the one used by Bretherton et al. (2005) [i.e., the NCAR Community Climate Model version 3 (CCM3; Kiehl et al. 1998]. In both cases, precipitating condensates are assumed to be radiatively negligible because of their large effective radii, so that only the condensates that are nonprecipitating (clouds) affect the radiative cooling rates.

Most simulations are initialized with horizontally homogeneous profiles of potential temperature and water

vapor mixing ratio from a mean tropical sounding with similar SST [average soundings from the Global Atmospheric Research Program (GARP) Atlantic Tropical Experiment (GATE) phase III (Houze and Betts 1981)]. To initiate convection, white noise is added to the dry static energy field in the lowest five levels of the model, with amplitude 0.1 K in the lowest level linearly decreasing to 0.02 K in the fifth level. To determine if the system exhibits hysteresis (section 4), we also perform runs starting from aggregated initial conditions (Fig. 6b); the initial potential temperature profile is the same as before, but the water vapor mixing ratio is initialized as a "moist bubble" in the center of the domain: specifically, at the first model level ($z = 37.5$ m), it decreases linearly from 0.016 kg kg^{-1} in the center of the domain to 0.006 kg kg^{-1} at a distance of $L/4$ (where L denotes the domain size), beyond which it is everywhere equal to 0.006 kg kg^{-1}. This initial horizontal profile decreases exponentially with height, with a height scale of 3 km.

Additional sensitivity runs are performed in section 5 to help interpret the results. These additional simulations are listed in Table 1. Specifically, in each run we horizontally homogenize or zero various fields in order to address the relative role played by different feedbacks in the onset of self-aggregation.

3. Properties of the self-aggregated state: Upgradient moist static energy transport

The self-aggregation of convection on large domains is illustrated in Fig. 1, which shows instantaneous snapshots of clouds and near-surface temperatures after
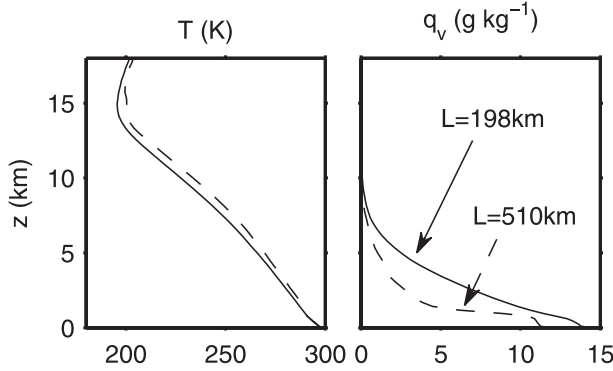
FIG. 3. Domain-averaged temperature T and water vapor mixing ratio q_v averaged over the last 10 days (days 51–60) of a run in two simulations with the same resolution $dx = 2$ km, but different domain sizes $L = 198$ (solid) and 510 km (dashed). Convection self-aggregates when the domain is large (Figs. 1b and 2b,d), which yields warmer and drier conditions.

60 days of run in two simulations with the same resolution (2 km) but different domain sizes (198 and 510 km). Figure 2 shows the daily mean precipitable water and outgoing longwave radiation in these two simulations. The small-domain run reaches radiative–convective equilibrium in about 30 days (after 30 days, variations in the domain-averaged daily mean precipitable water are less than 4%). The end climate is a state of somewhat disorganized convection (Figs. 1a and 2a,c). The large-domain run looks quite different; convection quickly self-aggregates (within a few days), eventually leading to an atmospheric state with one convectively active moist region surrounded by very dry air (Figs. 1b and 2b,d).

The thermodynamic and radiative properties are strongly affected by self-aggregation. In the run that self-aggregates, the dry region is extremely dry, much drier than anywhere in the run that results in disorganized radiative–convective equilibrium (cf. Figs. 2a,b). In the disorganized state parcels do not subside very far before they are moistened by a convective event; in the aggregated state, subsidence in the dry region is rarely interrupted by a moistening event. Consequently, the outgoing longwave radiation in the dry region comes from low levels that have high temperatures, yielding stronger radiative cooling to space than in the run that does not aggregate (cf. Figs. 2c,d). The domain-averaged vertical profiles of temperature and humidity (Fig. 3) also indicate much drier conditions with self-aggregation. As in Bretherton et al. (2005), we find that aggregation is accompanied by significant warming. This is due to high near-surface humidity in the convecting region, which leads to warmer moist adiabatic lapse rates there, and these warmer temperatures are impressed on the whole domain through the propagation of internal gravity waves.

Bretherton et al. (2005) studied the impact of self-aggregation on the energy transport and pointed out an upgradient energy transport when convection self-aggregates. The relevant energy in this model is the frozen moist static energy (MSE), since it is conserved during moist adiabatic processes in the model, including the freezing and melting of precipitation:

$$\mathrm{MSE} \equiv c_p T + gz + L_v q_v - L_f q_i, \qquad (1)$$

where c_p denotes the isobaric specific heat of dry air, T temperature, g gravitational acceleration, z height, L_v latent heat of vaporization, q_v water vapor mixing ratio, L_f latent heat of freezing, and q_i mixing ratio of all ice phase condensates (precipitating and nonprecipitating). The vertically integrated moist static energy budget, neglecting subgrid-scale fluxes, is (Khairoutdinov and Randall 2003; Bretherton et al. 2005)

$$\frac{d}{dt} \int \mathrm{MSE} = \mathrm{LHF} + \mathrm{SHF} + \Delta Q_r + C_{\mathrm{MSE}}, \qquad (2)$$

where the integral sign denotes vertical integration weighted by the reference density profile used in the anelastic governing equations, LHF and SHF denote the latent and sensible heat fluxes at the surface, ΔQ_r the radiative cooling lost by the atmospheric column at the top of atmosphere and at the surface, and C_{MSE} the vertically integrated horizontal convergence of MSE. Following Bretherton et al. (2005), the adiabatic term C_{MSE} in (2) is computed as a residual from this equation given the other terms rather than from infrequently stored three-dimensional fields. The variability of moist static energy is largely dominated by the variability of water vapor, so that the distribution of $\int \mathrm{MSE}$ looks very similar to the distribution of precipitable water shown in Figs. 2a and 2b. Therefore in the text, we equivalently refer to low moist static energy columns as dry columns, and to high moist static energy columns as moist columns.

Figure 4 compares the various terms of the moist static energy budget (2) in the small-domain run that does not self-aggregate (Fig. 4a) and in the large-domain run that does (Fig. 4b). Shown are time tendencies [left-hand side of (2)], diabatic contributions (surface and radiative fluxes), and adiabatic contributions C_{MSE}, as a function of column MSE (all the quantities shown on Fig. 4 are departures from domain averages). Our goal is to understand the onset of self-aggregation, so we look at early times of the simulation, namely days 6–10.

The diabatic term is a positive feedback (i.e., there is more cooling from the dry, low-energy region), but this is true whether the run aggregates or not. The difference between the two runs is the contribution from the
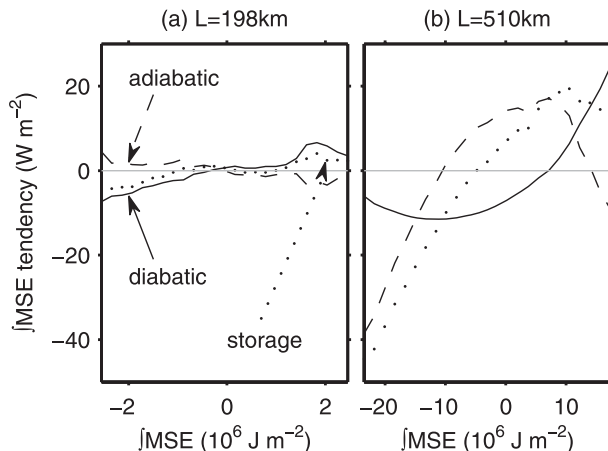
FIG. 4. Various terms in the moist static energy budget (2) in two simulations (a) without and (b) with self-aggregation. Shown are time averages from day 6 to day 10, as a function of vertically integrated MSE. All of the quantities shown (moist static energy on the x axis and moist static energy tendencies on the y axis) are departures from domain averages.

adiabatic term. In the run with disorganized convection, there is a downgradient horizontal transport of moist static energy, from the high-energy columns to the low-energy columns. The result is a time tendency that has similar values in all of the columns. In the self-aggregated run, on the other hand, the horizontal transport tends to be upgradient (i.e., from the low-energy columns to the high-energy columns), except at the highest column MSE. This results in larger moist static energy decreases in the dry, low-energy columns. This is consistent with Bretherton et al. (2005), who also find an upgradient horizontal transport of moist static energy with self-aggregation. Comparison with the run that does not self-aggregate shows that this upgradient moist static energy transport is specific to the run with self-aggregation.

4. Sensitivity of self-aggregation to resolution and domain size

Given this strong impact of self-aggregation on thermodynamic, radiative, and energy transport properties, it is important to understand its sensitivity to various parameters in the cloud-resolving model. We focus on domain size, following Bretherton et al. (2005) and Emanuel and Khairoutdinov (2010), who have shown that self-aggregation is favored by large domains, and on horizontal resolution. To initiate the resolution study, we start a new simulation similar to the run shown on Fig. 2 ($dx = 2$ km, $L = 510$ km) but with twice the number of points and half the grid spacing so that the domain size remains the same ($dx = 1$ km, $L = 510$ km).

Self-aggregation does not occur when we use a finer resolution (Fig. 5).

To check if this result is robust, we look at a wide range of resolutions and domain sizes and summarize our results in Fig. 6a. The runs that self-aggregate are represented as red circles, while the runs with disorganized convection are shown with black crosses. We check self-aggregation by looking at daily mean precipitable water after 30 days of run, although it typically only takes a few days for the convection to self-aggregate (Fig. 7). As before, all the runs are started from homogeneous initial conditions with added random noise to initiate the convection. It is clear that self-aggregation only occurs on large domains ($L \geq 200$ km) and at coarse resolutions ($dx \geq 2$ km).[1]

This system exhibits hysteresis [as pointed out by Emanuel and Khairoutdinov (2010)]. We start new runs, but with initial conditions that are aggregated. We initialize the run with a moist bubble in the center of the domain (see section 2 for more details) and check if the run disaggregates or remains aggregated after 100 days of run. The results are shown in Fig. 6b. In this case, the simulations need to run for a longer period since it can take quite long (over 80 days) for a run to disaggregate (see Fig. 8 for the time that a run takes to disaggregate as a function of resolution and domain size). In fact, we limit our runs to 100 days, so "remains aggregated" should be understood as "remains aggregated after 100 days." Even with this caveat, the fact that the convection remains aggregated for as long as 100 days requires explanation, since this time scale is longer than the typical equilibrium time of the radiative–convective model. We see that there is indeed hysteresis: self-aggregation can now occur at very fine resolutions ($dx = 500$ m) as long as the domain size is large enough ($L \geq 200, 300$ km). In fact, the ability of an aggregated state to remain aggregated appears to be less sensitive to resolution than the ability of aggregation to form from a more homogeneous state.

It may seem surprising that one of the runs ($dx = 4$ km, $L = 196$ km) does self-aggregate when started from homogeneous initial conditions but disaggregates when started from aggregated initial conditions. Since this simulation is very close to the boundary between aggregated and disorganized runs (gray boundary in Fig. 6), we expect its behavior to be highly sensitive to the details of the initial conditions. The results for this run are therefore likely due to the way we initialize the initially aggregated

---

[1] Preliminary results show that self-aggregation can occur with a horizontal resolution of 1 km if the domain size is 1024 km (M. Khairoutdinov 2011, personal communication).
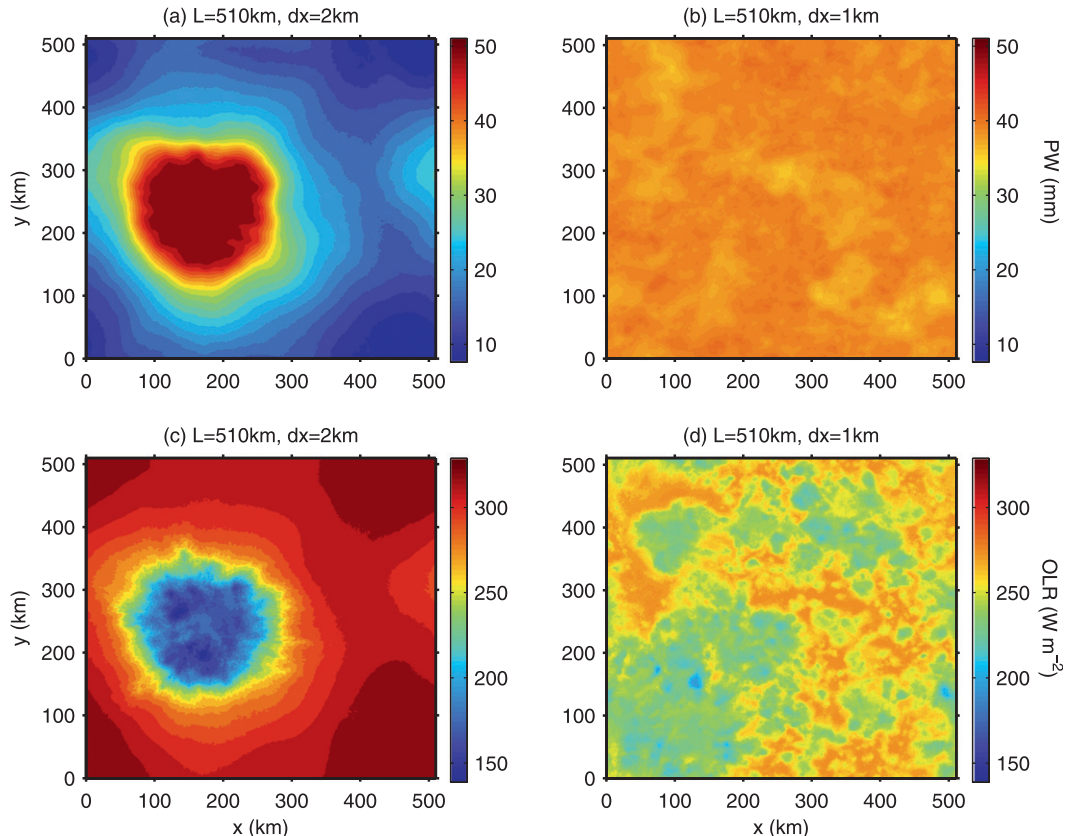
FIG. 5. As in Fig. 2, but for two runs having the same domain size and different resolutions.

run (i.e., to the details of the initial moist bubble described in section 2). The exact location of the gray boundary in Fig. 6 should be thought of as fuzzy, since it may be sensitive to the details of the initial condition [such as the value of the moisture field inside and outside the bubble, its size, and the fact that we use a moist bubble instead of a ''moist cold bubble,'' which would be more consistent with the aggregated state (Fig. 1b)]. Our idealized initial condition is sufficient to confirm that the system exhibits hysteresis (Fig. 6). We now return to simulations with homogeneous initial conditions and use various sensitivity runs to investigate the mechanism responsible for self-aggregation.

5. Mechanism responsible for self-aggregation: Role of longwave cooling from low clouds

a. Sensitivity runs: Role of longwave cooling from low clouds

What is the feedback responsible for self-aggregation and concomitant upgradient transport of moist static energy discussed in section 3? To answer this question, we perform sensitivity runs, listed in Table 1, in which

we successively turn off various feedbacks that could be responsible for self-aggregation. These include the interaction between convection and surface fluxes, as well as the interaction between convection and radiative cooling. The former is turned off by horizontally homogenizing surface fluxes at each time step (SFC-homog); the longwave (shortwave) interactive radiative cooling is turned off by horizontally homogenizing the longwave (shortwave) radiative cooling rate at each time step and at each height [LW-homog (SW-homog)]. We perform these sensitivity runs at various resolutions and domain sizes near $dx = 2$ km and $L = 250$ km. The results are summarized in Fig. 9; as in Fig. 6a, we check self-aggregation by looking at daily mean precipitable water after 30 days of run. Homogenizing the surface fluxes or the shortwave radiative cooling does not prevent self-aggregation, but homogenizing the longwave radiative cooling does: we have found no self-aggregation in LW-homog regardless of the domain size or resolution. It is therefore the interactive longwave radiative cooling that is responsible for the aggregation of convection. (There is still hysteresis in the runs with homogenized shortwave cooling and surface fluxes).
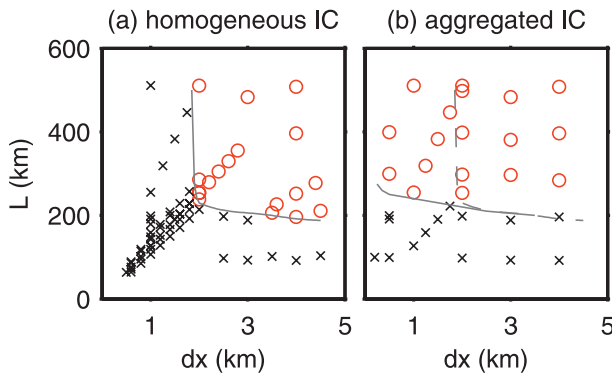
FIG. 6. Simulations with various resolutions dx and domain sizes L. (a) The runs are started from homogeneous initial conditions with added small random perturbations to initiate the convection and are run to 30 days. (b) The runs are started from aggregated initial conditions ("moist bubble" in the center of the domain) and are run to 100 days. Simulations that are self-aggregated at the end of the run are represented as red circles, while those with disorganized convection at the end of the run are shown with black crosses. A gray line is added at the boundary between aggregated and disorganized runs. The gray line from (a) is repeated as a dashed gray line in (b) to ease comparison.

FIG. 7. Time evolution of the hourly mean ΔPW (where Δ is the difference between the 75th and the 25th percentiles, and PW denotes precipitable water) in simulations started from homogeneous initial conditions, with the same number of points ($N = 128$) and different resolutions (from 0.5 to 2.8 km). The runs that aggregate are shown with solid lines, and the runs that do not aggregate are shown with dashed lines. Self-aggregation is associated with larger variability of PW (Fig. 2). While 30 days might not be long enough to reach the fully equilibrated aggregated climate in all the runs, it is sufficient to determine if a run spontaneously self-aggregates.

Despite the fact that neither shortwave interactive radiation nor inhomogeneous surface fluxes is crucial for self-aggregation in this model, both impact the aggregation. Shortwave interactive radiation opposes self-aggregation while inhomogeneous surface fluxes favor it. The former is due to the fact that moist regions have more clouds, leading to more shortwave cooling. So interactive shortwave radiation extracts energy from the high-energy columns, providing a negative feedback on self-aggregation. Surface fluxes, on the other hand, favor self-aggregation. This is because, as we will see in section 5b, the upgradient moist static energy transport is largely due to a near-surface flow from the dry to the moist region (Fig. 11b), which exports near-surface high-energy air from the dry columns. Surface evaporation enhances this near-surface export of high-energy air from the dry columns, providing a positive feedback on self-aggregation. So both inhomogeneities in surface fluxes and in shortwave radiative cooling impact the boundary between aggregated and nonaggregated runs (gray line in Fig. 6), yet neither shortwave cooling nor surface fluxes is crucial for self-aggregation; the important feedback is the interactive longwave cooling. This is not inconsistent with Bretherton et al. (2005), who find that self-aggregation disappears when surface fluxes are homogenized. We interpret their simulations as being near the self-aggregation boundary, so the enhancement from surface fluxes is needed to obtain self-aggregation. Based on our results, we infer that with a larger domain, or with coarser resolution, Bretherton et al. (2005) would
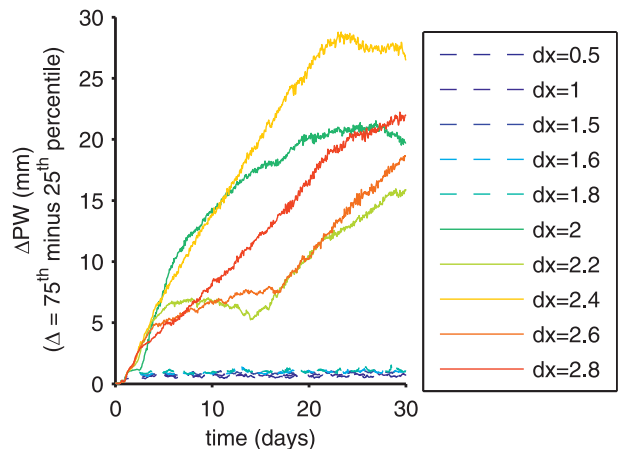
have obtained self-aggregation even with homogenized surface fluxes.

Determining the exact location of the boundary in each case in Figs. 9a–d, or if the boundary is in fact fuzzy, would require a more careful computation. But for our purpose, Fig. 9 is consistent with the qualitative results that 1) there is no self-aggregation with horizontally homogenized longwave cooling regardless of the domain size or resolution, 2) shortwave interactive radiation opposes self-aggregation, and 3) inhomogeneous surface fluxes favor self-aggregation.

We go one step further and separately investigate the contributions from water vapor, low clouds, and high clouds to the longwave radiative cooling. This is achieved by starting three additional simulations that all have homogeneous initial conditions, a resolution of 3 km, a domain size of 381 km, homogenized surface fluxes, and shortwave cooling, but which have different longwave cooling (Table 1). In the first simulation, we homogenize at each time step and height the amount of water vapor that enters the computation of the longwave cooling. In the second (third) simulation, we remove the contribution from the low (high) clouds to the longwave cooling by zeroing at each time step and height the amount of liquid (ice) condensates that enters the computation of the longwave cooling. The results are shown in Fig. 10. It is the interactive longwave radiation
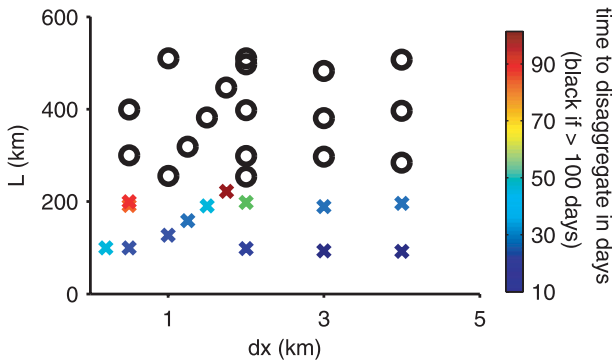
FIG. 8. Time (days) that the runs started from aggregated initial conditions (shown in Fig. 6b) take to disaggregate. Black circles indicate the runs that are still aggregated after 100 days of run. It typically takes longer to disaggregate with larger domains and with finer resolutions.

from liquid condensates (i.e., low clouds) that is responsible for self-aggregation.[2]

Looking back at Fig. 1, one may wonder why low clouds are absent from the dry regions in the simulation with aggregated convection; this is because, as we will see below (section 5c; Fig. 13), low clouds are needed for the onset of self-aggregation but not for its maintenance.

b. Circulation and mechanism responsible for self-aggregation

To clarify the role played by low clouds, we look at the circulation in more detail. The streamfunction Ψ introduced by Bretherton et al. (2005) quantifies the transport in height and energy space. Specifically, it is computed by ordering the columns with respect to their column moist static energy $\int MSE$ (index i) and calculating the corresponding vertical mass flux:

$$\Psi(i, z) = \Psi(i - 1, z) + \sum_{\int MSE \in (\int MSE_{i-1}, \int MSE_i]} w(z)\bar{\rho}(z),$$

$$(3)$$

with $\Psi(0, z) = 0$ for all z, where w denotes the vertical velocity and $\bar{\rho}$ the reference density profile used in the anelastic governing equations. In other words, $\Psi(i, z)$ is the total vertical mass flux over all the columns with $\int MSE \leq \int MSE_i$. This streamfunction does not represent

---

[2] The results are unchanged if we define low clouds as clouds below the 700-hPa pressure level ($z \leq 3$ km): zeroing the condensate amount that enters the longwave-cooling computation at levels below (above) the 700-hPa pressure level suppresses (does not suppress) aggregation. The results are also unchanged if instead of setting liquid/ice condensate amounts in the longwave radiation computation to zero, we horizontally homogenize them.
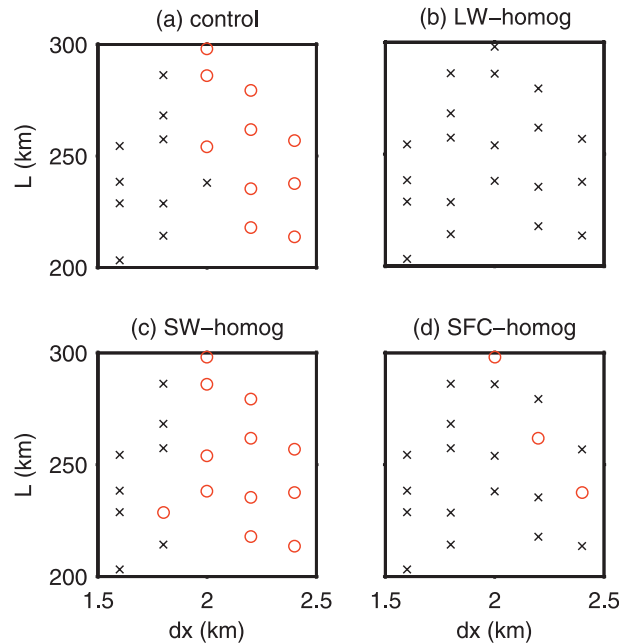

FIG. 9. Simulations with various resolutions dx and domain sizes L near $dx = 2$ km and $L = 250$ km. (a) The control runs are as in Fig. 6a (i.e., they are started from homogeneous initial conditions with added small random perturbations to initiate the convection and are run to 30 days). (b)–(d) The sensitivity runs are similar to the control runs, but with the addition of the longwave radiative cooling, the shortwave radiative cooling, and the surface fluxes homogenized, respectively (see Table 1). Simulations that are self-aggregated at the end of the run are represented as red circles, while those with disorganized convection at the end of the run are shown with black crosses.

circulation in physical space but is designed to allow the investigation of the transport between dry and moist regions.

To emphasize the effect of clouds, we compare the circulation in two runs that both have homogenized surface fluxes, shortwave radiative cooling, and longwave radiative cooling from water vapor. In addition, one of the runs has homogenized longwave radiative cooling from condensates and therefore does not self-aggregate. Figures 11a and 11b show the circulation without and with self-aggregation, respectively. Without self-aggregation, the circulation is as expected: there is upward motion in the moist region, horizontal divergence at high levels where the moist static energy is high, descent in the dry region, and a low-level return flow where the moist static energy is lower than in the upper-level outflow. This results in a net moist static energy transport from moist regions to dry regions, consistent with Fig. 4. With self-aggregation, on the other hand, the low-level circulation in the dry region is quite different. There is a secondary circulation near $z = 1$ km, with inflow of relatively
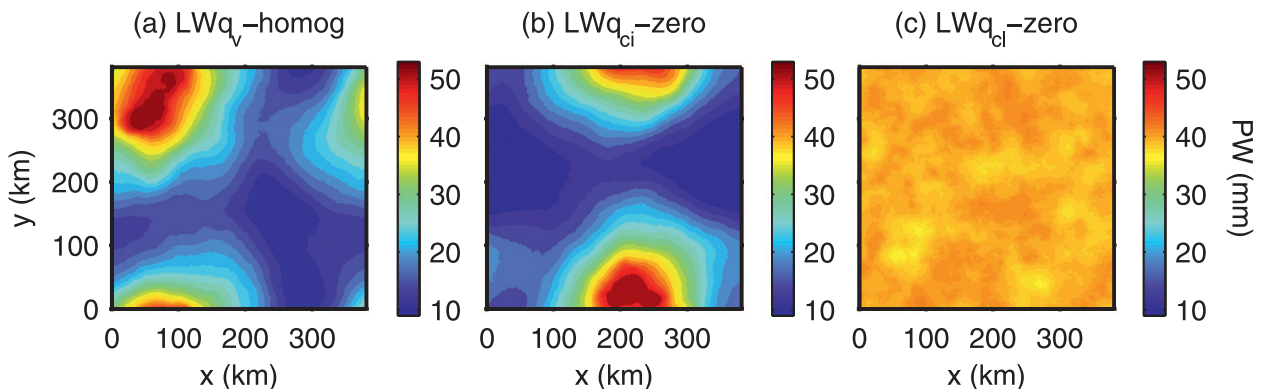
FIG. 10. Daily mean PW (mm) after 30 days in various sensitivity simulations (a) LWq_v-homog, (b) LWq_{ci}-zero, and (c) LWq_{cl}-zero described in Table 1.

low-energy air at these levels and a near-surface return flow of relatively high-energy air (below $z = 500$ m). This results in a net export of moist static energy from dry to moist regions. This is consistent with Bretherton et al. (2005), who also found a low-level secondary circulation with self-aggregation, leading to upgradient moist static energy transport.

Comparison of low clouds between the two runs in Fig. 11 (pink contours) makes clear how low clouds impact the circulation and hence the onset of self-aggregation. The secondary low-level circulation is due to the presence of low clouds in the dry region and to the associated low-level cooling (Fig. 11d). More precisely, we propose the following mechanism:

- the presence of low clouds in the dry region yields strong longwave cooling near the top of those clouds (around 1 km);
- this low-level cooling is balanced by subsidence warming; and
- by continuity, the descending air induces horizontal inflow of relatively low-energy air (between $z = 1$ and 2 km) into the dry region, which in turn forces a near-surface return flow of high-energy air (below $z = 500$ m) from the dry region. The resulting net transport of moist static energy is from dry to moist columns (i.e., upgradient).

We checked this result, namely that the export of moist static energy from the dry region is due to strong longwave cooling near the top of low clouds, by removing the longwave cooling from liquid condensates but only at low levels (below 1 km). It does indeed suppress self-aggregation. Removing the longwave cooling from liquid condensates above 2 km only, on the other hand, does not prevent self-aggregation.

We recognize that the extent to which the cooling from low clouds is balanced by subsidence and not by

turbulent mixing may be sensitive to the SGS parameterization. The SGS scheme used here is designed to parameterize the inertial-subrange part of the turbulent motions, but for low clouds and for the boundary layer, turbulent motions lie below the model resolutions, both horizontal and vertical, utilized here (e.g., Moeng et al. 2009; Bretherton et al. 1999). Therefore, the use of inertial-subrange-based SGS parameterizations likely distorts the boundary layer and low clouds in these simulations and in Bretherton et al. (2005) and Emanuel and Khairoutdinov (2010). On the other hand, we have examined runs with enhanced or weakened turbulent mixing (multiplying the SGS viscosity and diffusivity coefficients by constant factors) and found that our results were unchanged; so given this model's SGS closure, the sensitivity to the parameters in that closure may not be large.

The implication is that the dependence of self-aggregation on resolution and domain size is related to the sensitivity of the model's low clouds to these two parameters. Figure 12c shows the distribution of instantaneous near-surface relative humidity in the dry region after 1 day of run as a function of resolution and domain size. The near-surface relative humidity is sensitive to both resolution and domain size. More precisely, it increases with coarser resolution, due to both lower temperatures (Fig. 12a) and higher water vapor mixing ratios (Fig. 12b); the relationship between near-surface relative humidity and domain size is not as clear from Fig. 12. The runs that self-aggregate are shown as open circles. There is not an exact correspondence between the values of surface relative humidity and the aggregated runs, but in fact we would not expect one for several reasons. First, the fields shown in Fig. 12 are instantaneous fields and hence are somewhat noisy; second, they are computed near the surface whereas the relevant levels are near the top of low clouds; and third, they are computed after 1 day of

Ψ (black contours), qcl (pink contours), qci (white contours) and MSE (colors)

qcl (pink contours), qci (white contours) and Qr (colors)
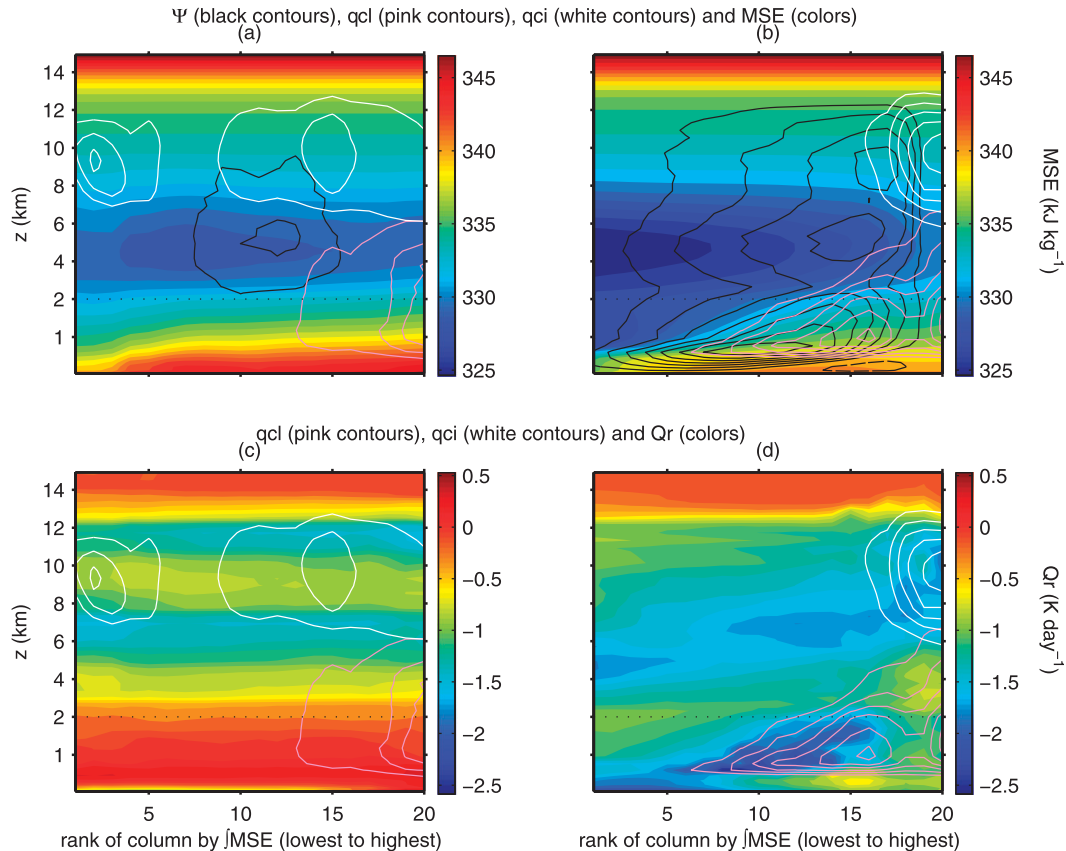

FIG. 11. (a),(b) Daily mean circulation and (c),(d) radiative cooling after 8 days (a),(c) in a run with disorganized convection and (b),(d) in a run that self-aggregates. Note the stretched vertical coordinate z below 2 km. In (a) and (b), black contours show the streamfunction Ψ (contour interval = 20 kg s^{-1} starting at ± 20 kg s^{-1}; solid for negative values and dashed for positive values) as a function of vertically integrated moist static energy and height z. In all panels, pink and white contours show nonprecipitating condensate amounts for liquid and ice, respectively (contour interval = 5 mg kg^{-1} starting at 5 mg kg^{-1}). The background colors represent moist static energy and radiative cooling in the top and bottom rows, respectively. Both runs have a domain size of 254 km, a resolution of 2 km, homogenized surface fluxes, homogenized SW radiative cooling, and homogenized longwave radiative cooling from water vapor. In addition, the simulation shown in (a) and (c) has homogenized radiative cooling from condensates and therefore does not self-aggregate.

run, which can correspond to different stages of the aggregation in different runs, since different runs do not aggregate at the same speed. Nevertheless, there is a clear indication that coarser resolutions yield higher relative humidities near the surface in the dry region (we find a similar relationship using daily mean liquid cloud water path instead of instantaneous surface relative humidity), thereby favoring low clouds and their associated low-level cooling and moist static energy export. This is consistent with Khairoutdinov et al. (2009), who also find an increase in low-cloud fractional area and low-cloud water with coarser horizontal resolutions. It is unsurprising that the distribution of condensates is sensitive to resolution and domain size. The turbulence controlling low clouds in these simulations is very far from resolved, and, in addition, low cloudiness and deep convection interact; and it is well known that the statistics of, for example, vertical velocity is sensitive to resolution and domain size in cloud-resolving models (Pauluis and Garner 2006; Parodi and Emanuel 2009). But it is unclear if and why near-surface relative humidity should increase with coarser horizontal resolutions or larger domains.

c. Hysteresis

The mechanism responsible for the onset of self-aggregation (longwave cooling from low clouds) may be different from the mechanism responsible for hysteresis and the maintenance of self-aggregation. Indeed, we performed an additional simulation LWq_{cl}-zero-delayed (Table 1; Figs. 13c,d) where the longwave radiative cooling from low clouds is only removed after 10 days of run.

(a) instantaneous Tsfc (K) at dry points after one day

(b) instantaneous Qsfc (g kg^{-1}) at dry points after one day

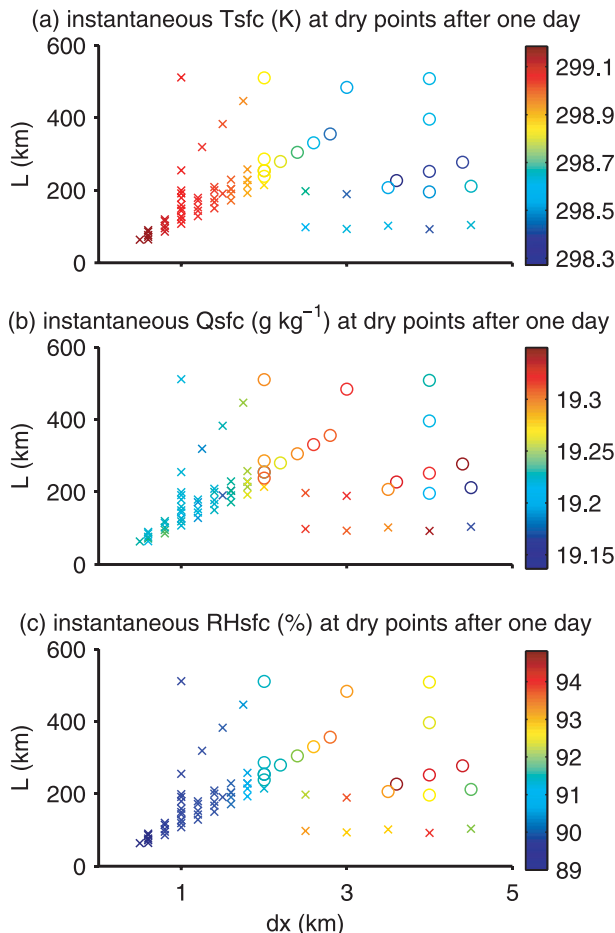(c) instantaneous RHsfc (%) at dry points after one day

FIG. 12. Instantaneous near-surface (at the first model level $z = 37.5$ m) (a) temperature, (b) water vapor mixing ratio, and (c) relative humidity after 1 day of run averaged over dry points (defined as precipitable water below its 50th percentile), as a function of resolution and domain size. Open circles correspond to runs that self-aggregate.

The convection remains aggregated even when the longwave cooling from low clouds is removed (Fig. 13d). Nevertheless, if we homogenize the total longwave radiative cooling after 10 days of run, the aggregation is suppressed (Figs. 13g,h). This seems to indicate that, although interactive longwave cooling from low clouds is necessary for the onset of self-aggregation, once the aggregated climate is reached, the strong clear-sky low-level radiative cooling in the dry region (due to the warm and dry conditions there) is sufficient to maintain the convective aggregation. In both cases (low-cloud or clear-sky radiative cooling), the low-level radiative cooling in the dry region yields a secondary circulation (Fig. 11b) that is responsible for the upgradient transport of moist static energy. More work is desirable to investigate in detail this hysteresis and the properties of the aggregated equilibrium climate.

d. Area of the aggregated region

An interesting question is what sets the properties of the aggregated climate, in particular the area of the aggregated convecting region. We only ran the simulations from homogeneous initial conditions to 30 days. This is enough to determine if a run spontaneously self-aggregates, but not necessarily to reach the fully equilibrated aggregated climate. It is therefore not easy to define the area of the aggregated region since it might change with time if the steady state had not yet been reached after 30 days; also it requires a definition of the aggregated region that involves arbitrary choices (e.g., based on a threshold value for outgoing longwave radiation or precipitable water, which requires the choice of a threshold value). Nevertheless we extended some of our runs to 60 days, and for those runs that aggregated and reached a steady state in 60 days we defined the area of the aggregated region based on various threshold values for precipitable water (we note in passing that all of our runs have only one aggregated region). We could not find a correlation between the latter and domain size or resolution. Neither did we find a correlation between the strength of the aggregation (defined as the difference between the 25th and the 75th percentiles of precipitable water) and domain size or resolution.

6. Conclusions

We use a three-dimensional cloud-resolving model to investigate in detail the self-aggregation of convection in nonrotating, doubly periodic simulations. Self-aggregation is known to occur only on large domains; we also find that it is sensitive to the resolution. When started from homogeneous initial conditions, convection only self-aggregates at coarse resolutions ($dx \geq 2$ km). The system exhibits hysteresis, so that when started from aggregated initial conditions, self-aggregation occurs even at the finest resolution ($dx = 500$ m) used in our study. This implies that if the large-scale conditions drive the aggregation of convection, convection will remain aggregated, which has consequences for the thermodynamic and radiative properties at large scales.

The exact values of resolution and domain size at which convection starts to self-aggregate are impacted by inhomogeneities in surface fluxes and in shortwave radiative cooling (shortwave interactive radiation opposes self-aggregation while inhomogeneous surface fluxes favor it), but neither of them is crucial for self-aggregation. The important feedback in this model is the interactive longwave cooling (there is no self-aggregation with horizontally homogenized longwave cooling regardless of the domain size or resolution). Specifically, the longwave
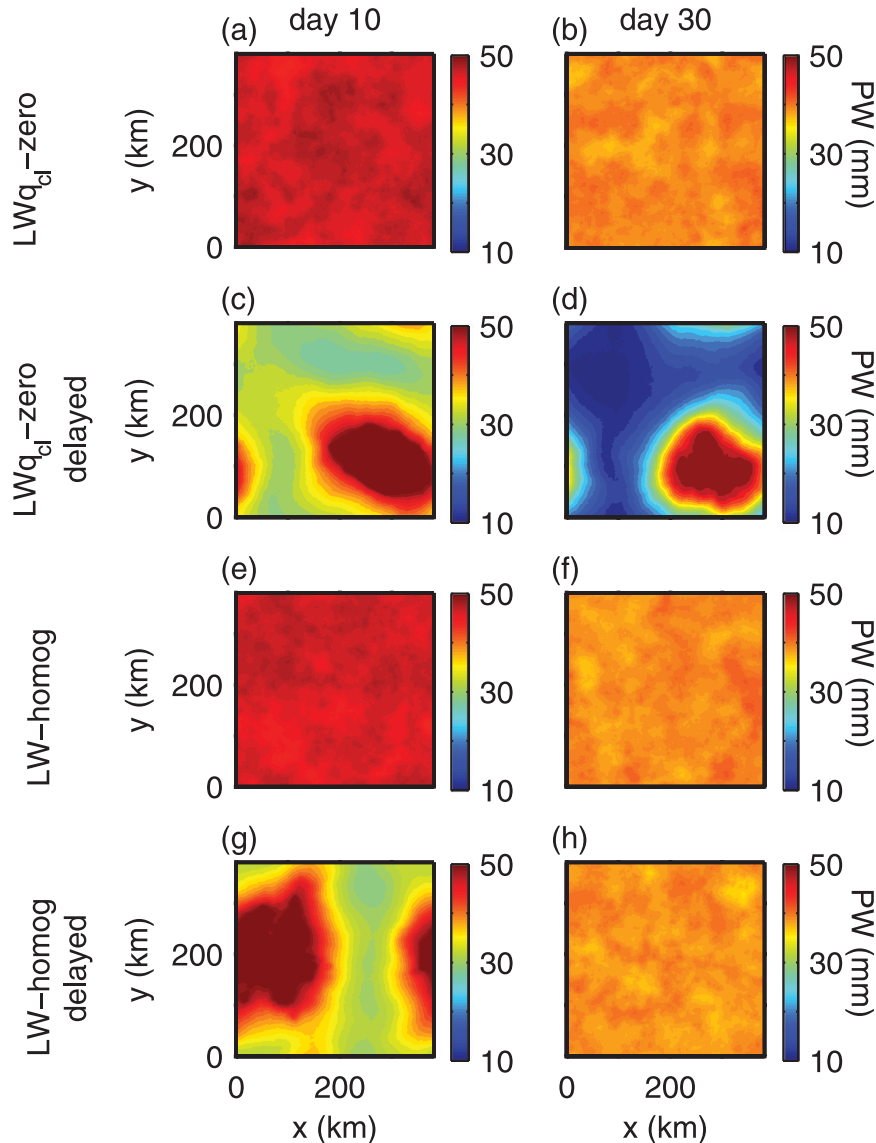
FIG. 13. Daily mean PW after (left) 10 and (right) 30 days in various sensitivity simulations with the same resolution and domain size (coarse and large enough to yield self-aggregation) with different radiative cooling as described in Table 1. (a),(b) Results from run LWq_{cl}-zero where the longwave cooling from low clouds is removed, which suppresses the aggregation as expected from Fig. 10c. (c),(d) As in (a),(b), but the longwave cooling from low clouds is only removed after day 10; in that case convective aggregation persists even when the longwave cooling from low clouds is removed in (d). (e),(f) A simulation with homogenized longwave cooling, which does not aggregate as expected from Fig. 9b. (g),(h) As in (e),(f), but the longwave cooling is only homogenized after day 10; homogenizing the total longwave radiative cooling after day 10 suppresses the aggregation in (h).

cooling near the top of low clouds in dry regions is responsible for the onset of self-aggregation: the concomitant subsidence forces low-level inflow (around $z = 1$ km) and near-surface outflow (below $z = 500$ m) from dry regions, resulting in a net export of moist static energy from regions with low moist static energy. This up-gradient moist static energy transport is the positive

feedback responsible for the onset of self-aggregation. The sensitivity of self-aggregation to domain size and resolution comes from the sensitivity of the distribution of low clouds to these two parameters.

The mechanism responsible for the onset of self-aggregation (longwave cooling from low clouds) may be different from the mechanism responsible for hysteresis

and the maintenance of self-aggregation (longwave clear-sky cooling). Low clouds are needed for the onset of self-aggregation, but once the aggregated climate is reached, the strong clear-sky radiative cooling in the dry region (due to the warm and dry conditions there) is sufficient to maintain the convective aggregation. In both cases (low-cloud or clear-sky longwave radiative cooling), the low-level radiative cooling in the dry region yields a secondary circulation that is responsible for the upgradient transport of moist static energy.

The relevance of self-aggregation to observed convective organization (mesoscale convective systems, mesoscale convective complexes, etc.) requires further investigation. Based on its sensitivity to resolution (Fig. 6a), it may be tempting to see self-aggregation as a numerical artifact that occurs at coarse resolutions, whereby low-cloud radiative feedback organizes the convection. Nevertheless, it is not clear that self-aggregation would not occur at fine resolution if the domain size were large enough. Furthermore, the hysteresis (Fig. 6b) increases the importance of the aggregated state, since it expands the parameter span over which the aggregated state exists as a stable climate equilibrium. The existence of the aggregated state appears to be less sensitive to resolution than the self-aggregation process. It is also possible that our results are sensitive to the value of the sea surface temperature; indeed, Emanuel and Khairoutdinov (2010) find that warmer sea surface temperatures tend to favor the spontaneous self-aggregation of convection.

Current convective parameterizations used in global climate models typically do not account for convective organization. More two-dimensional and three-dimensional simulations at high resolution are desirable to better understand self-aggregation, and convective organization in general, and its dependence on the subgrid-scale closure, boundary layer, ocean surface, and radiative scheme used. The ultimate goal is to help guide and improve current convective parameterizations. Promising results from studies with intermediate resolution (Su et al. 2000) or using superparametrizations (two-dimensional cloud-resolving models embedded in coarse global climate model; e.g., Benedict and Randall 2009; Tao et al. 2009; Tao and Moncrieff 2009) that allow for some convective organization have shown that the latter can strongly impact large-scale properties, including the hydrological cycle.

REFERENCES

Benedict, J. J., and D. A. Randall, 2009: Structure of the Madden–Julian oscillation in the superparameterized CAM. *J. Atmos. Sci.,* **66,** 3277–3296.

Bretherton, C. S., and Coauthors, 1999: An intercomparison of radiatively driven entrainment and turbulence in a smoke cloud, as simulated by different numerical models. *Quart. J. Roy. Meteor. Soc.,* **125,** 391–423.

——, P. N. Blossey, and M. Khairoutdinov, 2005: An energy-balance analysis of deep convective self-aggregation above uniform SST. *J. Atmos. Sci.,* **62,** 4273–4292.

Collins, W. D., and Coauthors, 2006: The formulation and atmospheric simulation of the Community Atmosphere Model version 3 (CAM3). *J. Climate,* **19,** 2144–2161.

Emanuel, K. A., 1986: An air–sea interaction theory for tropical cyclones. Part I: Steady-state maintenance. *J. Atmos. Sci.,* **43,** 585–604.

——, 1994: *Atmospheric Convection.* Oxford University Press, 580 pp.

——, and M. F. Khairoutdinov, 2010: Aggregated convection and the regulation of tropical climate. *Extended Abstracts, 29th Conf. on Hurricanes and Tropical Meteorology,* Tucson, AZ, Amer. Meteor. Soc., P2.69. [Available online at http://ams.confex.com/ams/29Hurricanes/techprogram/paper_168418.htm.]

Grabowski, W. W., and M. W. Moncrieff, 2001: Large-scale organization of tropical convection in two-dimensional explicit numerical simulations. *Quart. J. Roy. Meteor. Soc.,* **127,** 445–468.

——, and ——, 2002: Large-scale organization of tropical convection in two-dimensional explicit numerical simulations: Effects of interactive radiation. *Quart. J. Roy. Meteor. Soc.,* **128,** 2349–2375.

——, and ——, 2004: Moisture–convection feedback in the tropics. *Quart. J. Roy. Meteor. Soc.,* **130,** 3081–3104.

Held, I. M., R. S. Hemler, and V. Ramaswamy, 1993: Radiative-convective equilibrium with explicit two-dimensional moist convection. *J. Atmos. Sci.,* **50,** 3909–3909.

Holton, J. R., 2004: *An Introduction to Dynamic Meteorology.* 4th ed. Academic Press, 535 pp.

Houze, R. A., Jr., and A. K. Betts, 1981: Convection in GATE. *Rev. Geophys. Space Phys.,* **19,** 541–576.

Khairoutdinov, M. F., and D. A. Randall, 2003: Cloud-resolving modeling of the ARM summer 1997 IOP: Model formulation, results, uncertainties, and sensitivities. *J. Atmos. Sci.,* **60,** 607–625.

——, S. K. Krueger, C. H. Moeng, P. Bogenschutz, and D. A. Randall, 2009: Large-eddy simulation of maritime deep tropical convection. *J. Adv. Model. Earth Syst.,* **1** (15), doi:10.3894/JAMES.2009.1.15.

Kiehl, J. T., J. J. Hack, G. B. Bonan, B. A. Boville, D. L. Williamson, and P. J. Rasch, 1998: The National Center for Atmospheric Research Community Climate Model: CCM3. *J. Climate,* **11,** 1131–1149.

Moeng, C. H., M. A. LeMone, M. F. Khairoutdinov, S. K. Krueger, P. Bogenschutz, and D. A. Randall, 2009: The tropical marine boundary layer under a deep convection system: A large-eddy simulation study. *J. Adv. Model. Earth Syst,* **1,** (16), doi:10.3894/JAMES.2009.1.16.

Nesbitt, S. W., E. J. Zipser, and D. J. Cecil, 2000: A census of precipitation features in the tropics using TRMM: Radar, ice scattering, and lightning observations. *J. Climate,* **13,** 4087–4106.

Parodi, A., and K. A. Emanuel, 2009: A theory for buoyancy and velocity scales in deep moist convection. *J. Atmos. Sci.,* **66,** 3449–3463.

Pauluis, O., and S. Garner, 2006: Sensitivity of radiative–convective equilibrium simulations to horizontal resolution. *J. Atmos. Sci.,* **63,** 1910–1923.

Robe, F. R., and K. A. Emanuel, 2001: The effect of vertical wind shear on radiative-convective equilibrium states. *J. Atmos. Sci.,* **58,** 1427–1445.

Stephens, G. L., S. van den Heever, and L. Pakula, 2008: Radiative–convective feedbacks in idealized states of radiative–convective equilibrium. *J. Atmos. Sci.,* **65,** 3899–3916.

Su, H., C. S. Bretherton, and S. S. Chen, 2000: Self-aggregation and large-scale control of tropical deep convection: A modeling study. *J. Atmos. Sci.,* **57,** 1797–1816.

Tao, W.-K., and M. W. Moncrieff, 2009: Multiscale cloud system modeling. *Rev. Geophys.,* **47,** RG4002, doi:10.1029/2008RG000276.

——, and Coauthors, 2009: A multiscale modeling system: Developments, applications, and critical issues. *Bull. Amer. Meteor. Soc.,* **90,** 515–534.

Tompkins, A. M., 2001a: Organization of tropical convection in low vertical wind shears: The role of water vapor. *J. Atmos. Sci.,* **58,** 529–545.

——, 2001b: Organization of tropical convection in low vertical wind shears: The role of cold pools. *J. Atmos. Sci.,* **58,** 1650–1672.

——, and G. C. Craig, 1998: Radiative-convective equilibrium in a three-dimensional cloud-ensemble model. *Quart. J. Roy. Meteor. Soc.,* **124,** 2073–2097.

WCRP, 1999: Proceedings of a conference on the Toga Coupled Ocean–Atmosphere Response Experiment (COARE). WCRP-107, WMO Tech. Doc. 940, 416 pp.